The Astrophysical Journal, 768:52 (10pp), 2013 May 1 doi:10.1088/0004-637X/768/1/52

THE NATURE OF γ-RAY LOUD NARROW-LINE SEYFERT I GALAXIES PKS 1502+036 AND PKS 2004−447

Vaidehi S. Paliya[1,2], C. S. Stalin[1], Amit Shukla[1], and S. Sahayanathan[3]
[1] Indian Institute of Astrophysics, Block II, Koramangala, Bangalore 560 034, India; vaidehi@iiap.res.in
[2] School of Inter-Disciplinary and Trans-Disciplinary Studies, IGNOU, New Delhi 110 068, India
[3] Astrophysical Science Division, Bhabha Atomic Research Center, Mumbai 400 085, India
Received 2013 January 16; accepted 2013 March 8; published 2013 April 15

ABSTRACT

Variable γ-ray emission has been discovered in five radio-loud narrow-line Seyfert 1 (NLSy1) galaxies by the Large Area Telescope on board the *Fermi Gamma-ray Space Telescope*. This has clearly demonstrated that these NLSy1 galaxies do have relativistic jets similar to two other cases of γ-ray-emitting active galactic nuclei (AGNs), namely, blazars and radio galaxies. We present here our results on the multi-band analysis of two γ-ray-emitting NLSy1 galaxies, namely, PKS 1502+036 ($z = 0.409$) and PKS 2004−447 ($z = 0.240$), using archival data. We generate multi-band long-term light curves of these sources, build their spectral energy distribution (SED), and model them using a one-zone leptonic model. They resemble more the SEDs of the flat spectrum radio quasar (FSRQ) class of AGNs. We then compare the SEDs of these two sources with two other *Fermi*-detected AGNs along the traditional blazar sequence, namely, the BL Lac Mrk 421 ($z = 0.03$) and the FSRQ 3C 454.3 ($z = 0.86$). The SEDs of both PKS 1502+036 and PKS 2004−447 are found to be intermediate to the SEDs of Mrk 421 and 3C 454.3. In the γ-ray spectral index versus γ-ray luminosity plane, both these NLSy1 galaxies occupy a distinct position, wherein they have luminosity between Mrk 421 and 3C 454.3; however, their steep γ-ray spectra are similar to 3C 454.3. Their Compton dominance as well as their X-ray spectral slope also lie between Mrk 421 and 3C 454.3. We argue that the physical properties of both PKS 1502+036 and PKS 2004−447 are generally similar to blazars and intermediate between FSRQs and BL Lac objects and these sources thus could fit into the traditional blazar sequence.

Key words: galaxies: active – galaxies: Seyfert – gamma rays: galaxies – quasars: individual (PKS 1502+036, PKS 2004−447)

Online-only material: color figures

1. INTRODUCTION

The extragalactic sky in the high-energy γ-ray band is dominated by a special class of active galactic nuclei (AGNs) called blazars (Abdo et al. 2010a). These blazars which come under two sub-classes, namely, flat spectrum radio quasars (FSRQs) and BL Lac objects (see, for e.g., Urry & Padovani 1995), have similar broadband continuum properties, such as that they emit variable non-thermal emission over the entire electromagnetic spectrum. They both have flat radio spectra ($\alpha_r < 0.5$; $S_\nu \propto \nu^{-\alpha}$) at GHz frequencies, high optical polarization, exhibit a superluminal pattern at radio-frequencies, and also show rapid flux and polarization variations (Wagner & Witzel 1995; Andruchow et al. 2005). However, the distinction between FSRQs and BL Lac objects is made on the difference in the strength of their optical emission lines. BL Lac objects have weak optical emission lines with rest-frame equivalent widths less than 5 Å (Stocke et al. 1991; Stickel et al. 1991). The observed broadband emission of blazars is believed to originate from relativistic jets which are aligned closely to the observer (Begelman et al. 1984). Their spectral energy distribution (SED) shows two prominent and distinct peaks: the low-energy peak due to synchrotron emission, which lies between the far-infrared and the X-ray band, and the high-energy peak due to inverse Compton (IC) radiation, which lies in the MeV to GeV energy range. The seed photons for IC emission can be synchrotron photons themselves (synchrotron self-Compton, SSC; Konigl 1981; Marscher & Gear 1985; Ghisellini & Maraschi 1989) or photons external to the jet (external Compton, EC; Begelman & Sikora 1987; Melia & Konigl 1989; Dermer et al. 1992). The plausible sources of seed photons for EC can be the accretion disk (Dermer & Schlickeiser 1993; Boettcher et al. 1997), the broad-line region (BLR; Sikora et al. 1994; Ghisellini & Madau 1996), the dusty torus (Błażejowski et al. 2000; Ghisellini & Tavecchio 2008), the bulge of the host galaxy, or cosmic microwave background radiation (Ghisellini & Tavecchio 2009). In the γ-ray regime, FSRQs are more luminous and exhibit a softer spectral index than BL Lac objects (Abdo et al. 2009a). It has been noted by Fossati et al. (1998) and Ghisellini et al. (1998) that both FSRQs and BL Lac objects follow the so-called blazar sequence. However, recently Giommi et al. (2012) have argued that the existence of blazar sequence could be due to selection effects.

In addition to blazars which are dominating the γ-ray extragalactic sky, *Fermi* has also discovered variable γ-ray emission from five narrow-line Seyfert 1 (NLSy1) galaxies (Abdo et al. 2009b, 2009c; D'Ammando et al. 2012; Calderone et al. 2011). A few more NLSy1 sources are suspected to be γ-ray emitters, although the detection significance is still low (Foschini 2011). NLSy1 galaxies are a separate class of AGNs with peculiar properties. Their optical spectra are similar to the conventional broad-line Seyfert 1 galaxies except that they have narrow Balmer lines (FWHM (H_β) < 2000 km s^{-1}), and weak [O III] ([O III]/$H_\beta < 3$) and strong optical Fe II lines (Osterbrock & Pogge 1985; Goodrich 1989). They also have steep soft X-ray spectra (Boller et al. 1996; Wang et al. 1996; Leighly 1999a) and show rapid X-ray flux variations (Pounds et al. 1995; Leighly 1999b). These peculiar observational characteristics are attributed to them having low-mass black holes ($\sim 10^6$–$10^8\ M_\odot$) and accreting close to the Eddington limit (Peterson et al. 2000; Hayashida 2000; Grupe & Mathur 2004; Zhou et al. 2006; Xu et al. 2012). However, recently, Calderone

Table 1
List of the γ-NLSy1 Galaxies Monitored in This Work and the Results of the Analysis of About Four Years of *Fermi*-LAT Data

Name	R.A. (2000) (h m s)	Decl (2000) (d m s)	z[a]	M_B[a] (mag)	V[a] (mag)	α_R[b]	R[c]	$F_{0.1-300\,\mathrm{GeV}}$	Γ	TS	N_H[d]
(1)	(2)	(3)	(4)	(5)	(6)	(7)	(8)	(9)	(10)	(11)	(12)
PKS 1502+036	15:05:06.5	+03:26:31	0.409	−22.8	18.64	0.41	3364	5.15 ± 0.42	2.67 ± 0.06	419.28	3.93
PKS 2004−447	20:07:55.1	−44:34:43	0.240	−21.6	19.30	0.38	6358	1.66 ± 0.33	2.58 ± 0.12	67.67	3.17

Notes. Column information is as follows: (1) name; (2) right ascension; (3) declination; (4) redshift; (5) absolute B magnitude; (6) apparent V magnitude; (7) radio spectral index; (8) radio loudness parameter; (9) 0.1–300 GeV flux in units of 10^{-8} photons cm^{-2} s^{-1}; (10) photon index obtained from *Fermi*-LAT data analysis; (11) TS; and (12) N_H.
[a] Véron-Cetty & Véron (2010).
[b] Radio spectral index calculated using 6 cm and 20 cm flux densities given by Véron-Cetty & Véron (2010).
[c] Foschini (2011).
[d] Galactic absorption in units of 10^{20} cm^{-2} from Kalberla et al. (2005).

et al. (2012), using multi-wavelength data, have shown that radio-loud NLSy1 (RL-NLSy1) galaxies have black hole masses similar to blazars. These RL-NLSy1 galaxies comprising about 7% of the NLSy1 galaxy population exhibit a compact core–jet structure, flat/inverted radio spectra, high brightness temperature, and superluminal motion (Komossa et al. 2006; Doi et al. 2006). Recently, kiloparsec-scale radio structures are found in six RL-NLSy1 galaxies (Doi et al. 2012). The SEDs of some RL-NLSy1 galaxies are found to be similar to those of high-frequency-peaked BL Lac objects and some of them also show a hard X-ray component in their bright optical/UV state (Yuan et al. 2008). Though these characteristics are indicative of the presence of relativistic jets in these sources that are closely aligned to the observer, the detection of γ-rays in five of them has confirmed their presence (Abdo et al. 2009b, 2009c; D'Ammando et al. 2012), similar to the blazar class of AGNs. Also, it has recently been reported that the optical and infrared (IR) flux variations of some of these sources are similar to blazars (Liu et al. 2010; Paliya et al. 2013; Jiang et al. 2012; Maune et al. 2013). However, these similarities are at odds with the common belief that NLSy1 galaxies are hosted in spiral galaxies with low-mass black holes, while blazars with powerful relativistic jets are hosted in elliptical galaxies with high-mass black holes. Therefore, detailed studies of these sources will enable us to understand the physical properties of relativistic jets hosted in AGNs with low-mass central black holes and high accretion rates. In this work, we have carried out a detailed analysis of two such sources, namely, PKS 1502+036 and PKS 2004−447, to see (1) the similarities and/or differences of them vis-a-vis the blazars detected by *Fermi* and (2) their place in the traditional blazar sequence. A detailed analysis of these sources is presented here for the first time. Throughout this work, we adopt $\Omega_m = 0.27$, $\Omega_\Lambda = 0.73$, and Hubble constant $H_0 = 70$ km s^{-1} Mpc^{-1}.

2. SAMPLE

We have selected two of the five known γ-ray-emitting NLSy1 (γ-NLSy1) galaxies, namely, PKS 1502+036 and PKS 2004−447. They have intermediate redshifts when compared to other γ-NLSy1 galaxies. PKS 1502+036 has a very compact core on observations with the Very Large Array (Orienti et al. 2012; Kimball et al. 2011). However, when observed at 15 GHz using the Very Long Baseline Array at parsec scale resolution, it was found to have a core–jet structure (Orienti et al. 2012). This NLSy1 galaxy, with a central black hole mass of $\sim 4 \times 10^6\,M_\odot$, has a brightness temperature of $\sim 10^{12}$ K (Yuan et al. 2008). It is a faint but persistent γ-ray emitter (Calderone et al. 2011; Abdo et al. 2009c) and also shows intra-night optical variability (INOV; Paliya et al. 2013) and rapid IR variability (Jiang et al. 2012).

PKS 2004−447 has been classified as an NLSy1 galaxy by Oshlack et al. (2001) and Gallo et al. (2006), but Komossa et al. (2006) classify it as a narrow-line radio galaxy owing to the presence of weak Fe II lines in its optical spectra. It has a steep spectrum above 8.4 GHz (Orienti et al. 2012); however, it has a flat spectrum below 5 GHz (Healey et al. 2007). At 20 GHz, it shows a fractional polarization of 3.8% (Murphy et al. 2010). The general properties of both sources are given in Table 1.

3. DATA REDUCTION AND ANALYSIS

3.1. FERMI-Large Area Telescope

The *Fermi*-Large Area Telescope (LAT; Atwood et al. 2009) data used in this work were collected over the last four years of *Fermi* operation, from 2008 August 5 00:00:00 UT to 2012 July 24 00:00:00 UT. LAT photons of event class 2 between 100 MeV and 300 GeV were extracted from the *Fermi* Science Support Center[4] within a 30° circular region of interest centered around the position of the objects. Analysis of the data was performed with the LAT software package `ScienceTools v9r27p1` along with the use of post-launch instrument response functions P7SOURCE_V6 and the corresponding Galactic and isotropic diffuse background models. Additionally, a cut on the zenith angle ($<100°$) was applied in order to exclude the contamination from Earth's albedo. The spectral analysis was performed using an unbinned maximum likelihood method. The data were fitted with a simple power-law model. In the analysis, we consider the source to be detected if test statistic (TS) > 9. This corresponds to $\sim 3\sigma$ detection (Mattox et al. 1996). For TS < 9, 2σ upper limits were calculated. Systematic uncertainties in the flux were estimated as 10% at 0.1 GeV, 5% at 560 MeV, and 20% at 10 GeV and above.[5] Results of the average analysis are given in Table 1.

3.2. SWIFT (BAT, XRT, UVOT)

We have searched for the data from all three telescopes on board *Swift* (Gehrels et al. 2004), namely, the Burst Alert Telescope (BAT; Barthelmy et al. 2005) operating in the 15–150 keV band, the X-Ray Telescope (XRT; Burrows et al. 2005) operating in the 0.3–10 keV band, and the Ultra-Violet Optical Telescope

[4] http://fermi.gsfc.nasa.gov/ssc/data
[5] http://fermi.gsfc.nasa.gov/ssc/data/analysis/LAT_caveats.html

(UVOT; Roming et al. 2005) which can observe the sky in six filters, namely, *V, B, U, UVW1, UVM2,* and *UVW2*. We extracted all publicly available optical/UV/X-ray data for the sources from HEASARC archives. The data were analyzed using the latest *Swift* tools included in `HEASOFT v.6.12.0` together with calibration data files (CALDB) updated on 2012 April 2.

Both γ-NLSy1s could not be detected in the 15–150 keV band. We analyzed the XRT data using the XRTDAS software package developed at the ASI Science Data Center and distributed by HEASARC within the HEASoft package (v.6.12.0). Data were cleaned with standard filtering criteria and calibrated using the `xrtpipeline` task with default parameters and single-to-quadruple events (grades 1–12). We did not find any evidence of pile-up. Events for spectral analysis were selected within a circle of 50″ radius, centered on the source position, while the background was selected from a nearby source-free region with 100″ radius. To generate light curves, we first rebinned the spectrum to have at least one count per bin (using `grppha`) and then calculated the likelihood using C-statistics (Cash 1979). The data were fitted with an absorbed power-law model with Galactic absorption values taken from Kalberla et al. (2005). For light curve analysis, we have not corrected the XRT data for galactic absorption. For SED analysis, the individual XRT event files were combined together using the `XSELECT` package and the average spectrum was extracted from summed event files. Depending on the total detected counts, we grouped the spectrum so as to have at least 5 counts per bin for PKS 1502+036 and 15 counts per bin for PKS 2004−447. Model fitting was done using `XSPEC` (Arnaud 1996). Finally, the SED data were corrected for Galactic absorption and then binned appropriately for both sources.

Swift-UVOT has observed these sources in all six filters for most of the observations but not always. The UVOT data were integrated with the `uvotimsum` task and then analyzed with the `uvotsource` task. The source region was chosen as a circle of 5″ radius for optical filters and 10″ radius for UV, while the 1′ sized background region was extracted from nearby source-free regions. The observed magnitudes were de-reddened using the extinction laws of Cardelli et al. (1989) and converted to flux units using the zero points and conversion factors of the *Swift*-CALDB (Poole et al. 2008).

4. RESULTS

4.1. Multi-band Temporal Behavior

The long-term multi-band light curves of the two sources PKS 1502+036 and PKS 2004−447 are shown in Figures 1 and 2, respectively. In the γ-ray band, flux values were obtained over 30 day binning, whereas in the other bands, each flux point corresponds to one observation of *Swift*. For PKS 1502+036, only four sets of *Swift* data were available. As the data are sparse, no strong claims of variability could be made. However, a visual examination shows some hints of variability in the UVOT bands. In the γ-ray band, the source was mostly in the low activity state; however, it was found to be in a relatively bright state between MJD 55592 and 55622. It is also found to be variable at 15 GHz when observed from the Ovens Valley Radio Observatory (OVRO).[6]

For PKS 2004−447, the sparseness of the data precluded us from providing any estimates of the variability of the source. The visual examination of the light curves in the UVOT bands provides hints that the source has shown variability. The source has also shown significant variability in the X-ray band. When first observed on MJD 55696, its observed flux was $(4.42 \pm 1.23) \times 10^{-13}$ erg cm^{-2} s^{-1}, which increased by $\sim$3 times when observed again on MJD 55821 but diminished to $(5.36 \pm 2.20) \times 10^{-13}$ erg cm^{-2} s^{-1} when observed on MJD 56130. In the γ-ray band, the source was detected only in two epochs when analyzed using a 30 day binning. Comparing the counts at those two epochs, we find that the source has varied in flux.

4.2. X-Ray Spectral Fit

For PKS 1502+036, all *Swift*/XRT observations were integrated (global exposure = 19.25 ksec) and then fitted with an absorbed power law. We find the photon index, $\Gamma = 1.70 \pm 0.20$, the normalization at 1 KeV $= (4.49 \pm 0.67) \times 10^{-5}$ photons cm^{-2} s^{-1} keV^{-1}, and the integrated flux in the 0.3–10 keV energy band $= (2.90 \pm 0.69) \times 10^{-13}$ erg cm^{-2} s^{-1}.

When fitting an absorbed power-law model to the integrated data (global exposure = 45.89 ksec) of PKS 2004−447, we find $\Gamma = 1.53 \pm 0.09$ and the normalization at 1 keV $= (8.14 \pm 0.57) \times 10^{-5}$ photons cm^{-2} s^{-1} keV^{-1}. The flux in the 0.3–10 keV energy band $= (6.26 \pm 0.73) \times 10^{-13}$ erg cm^{-2} s^{-1}.

4.3. γ-Ray Spectral Variability Analysis

In Figure 3, we show the correlation of the 0.1–300 GeV flux against the γ-ray spectral slope for the source PKS 1502+036 when the 30 day time binning was used. The photon index values were obtained by fitting a power-law model to the *Fermi*-LAT data. When fitting the data using both the unweighted linear least-squares method and the weighted linear least-squares fit (which takes into account the errors on both the dependent and independent variables, Press et al. 1992), we found clear evidence of the "softening when brightening" kind of behavior. In the case of PKS 2004−447, we only have two detections at the epochs MJD 55232 and MJD 55802. The flux values at these two epochs are $(7.93 \pm 2.74) \times 10^{-8}$ and $(4.72 \pm 1.91) \times 10^{-8}$ photons cm^{-2} s^{-1}, respectively. The photon indices at MJD 55232 and MJD 55802 are 3.12 ± 0.38 and 2.56 ± 0.31. Thus, between the two epochs of detection, the γ-ray spectral index shows a "softening when brightening" trend. This behavior of the photon index is contradictory to the "harder when brighter" trend seen in the brightest FSRQ 3C 454.3 (Abdo et al. 2010b).

4.4. Spectral Energy Distribution

To investigate the physical characteristics of these sources, we have built optical/UV to γ-ray SEDs using quasi-simultaneous data. For PKS 1502+036, we have used the data sets between MJD 55800 and 56130, whereas for PKS 2004−447, the data sets spanning the period MJD 55680 and 56130 were used. These time periods are shown as vertical dashed lines in Figures 1 and 2 for PKS 1502+036 and PKS 2004−447, respectively. The derived flux values in optical/UV, X-ray, and γ-rays are given in Table 2. Both the SEDs were modeled using a simple one-zone leptonic emission model described in Sahayanathan & Godambe (2012). In this model, the emission region is assumed to be a spherical blob moving down the jet at a relativistic speed with a bulk Lorentz factor Γ. The emission region is filled with a broken power-law electron distribution

[6] http://www.astro.caltech.edu/ovroblazars/data/data.php

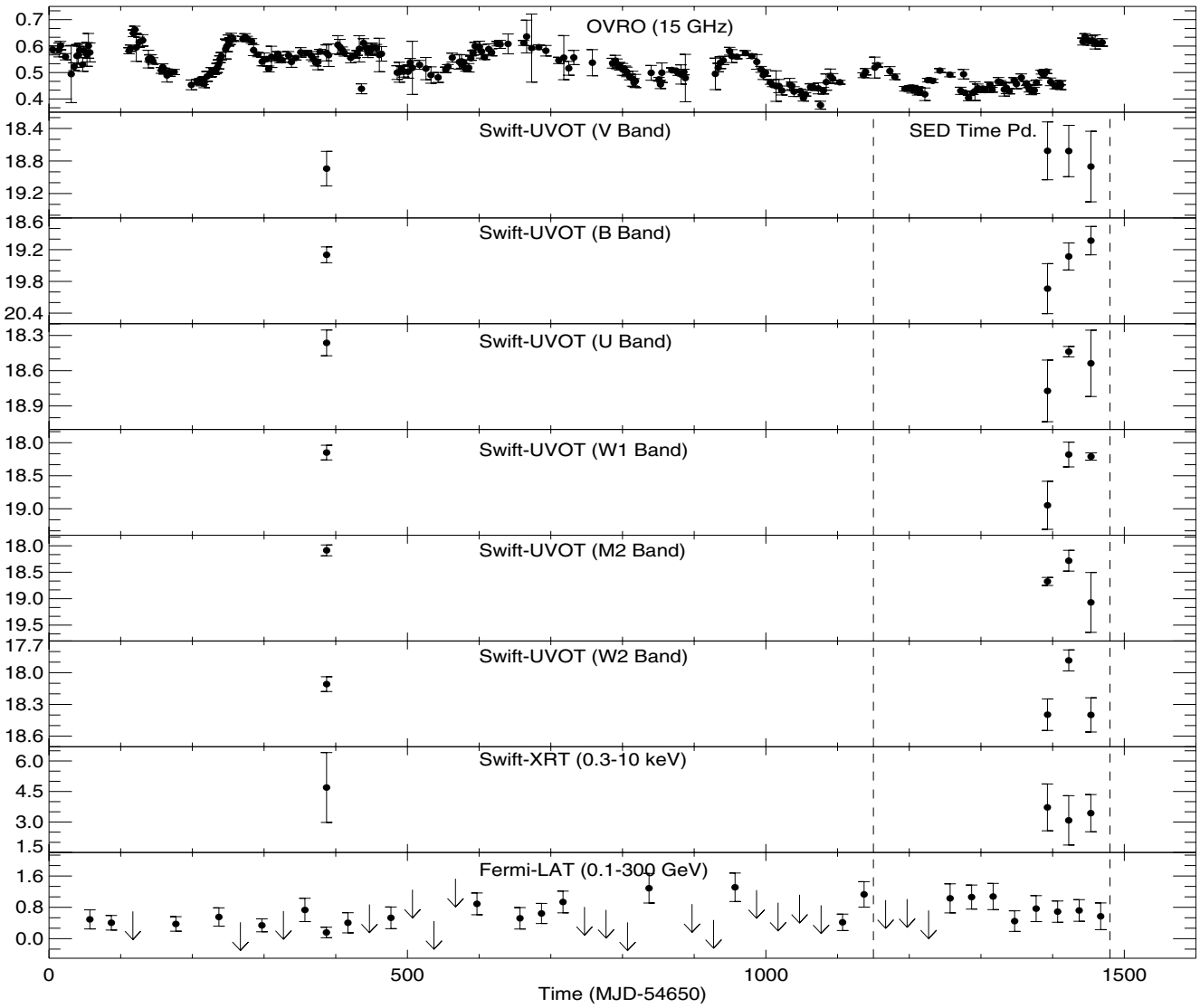

Figure 1. Multi-band light curves of PKS 1502+036. The OVRO data are in Jansky. UVOT data are in magnitude. XRT fluxes are in units of 10^{-13} erg cm^{-2} s^{-1}, while LAT γ-ray data have the unit of 10^{-7} photons cm^{-2} s^{-1}. Here, 95% upper limits are shown by vertical arrows. The dashed vertical line shows the time interval covered for SED modeling.

with indices p and q before and after the break energy, respectively. The particles lose their energy through synchrotron radiation in a randomly oriented magnetic field (B) and IC radiation. The target photons for the IC radiation are the synchrotron photons (SSC) and an external photon field. For simplicity, the external photon field is assumed to be a blackbody at temperature T* arising from a spherical shell covering the supermassive black hole and the emission region. Considering the magnetic field to be in equipartition with the relativistic particle distribution, the main parameters governing the SED can be deduced/constrained using the observed information available in the optical/X-ray and γ-ray energies. The kinetic power of the jet can then be calculated by assuming the inertia of the jet being provided by cold protons whose number density is equal to that of non-thermal electrons. This model does not take into account UV/optical emission from the accretion disk and X-ray emission from the hot corona. For the model fitting, we assume a variability timescale of $\sim$1 day, which is typically seen in the γ-ray light curves of blazars.

The resultant model fits to the SEDs for PKS 1502+036 and PKS 2004−447 are shown in Figure 4. The optical-UV flux can be reproduced by synchrotron emission and the X-ray flux by SSC emission. The explanation of the γ-ray flux as an outcome of the EC process demands the temperature of the external photon field to be 605 K in the case of PKS 1502+036 and 694 K for PKS 2004−447. The spectrum of this external photon field blackbody component with luminosities of 8.19 $\times$ 10^{43} erg s^{-1} and 6.26 $\times$ 10^{43} erg s^{-1} for PKS 1502+036 and PKS 2004−447, respectively, is shown in Figure 4. We compared the luminosity of this blackbody component with the observed luminosity (which is the sum of thermal and non-thermal components) in the Two Micron All Sky Survey (2MASS) and *WISE* bands and as expected they are lower than the observed luminosities. Also, the deduced temperatures are consistent with the temperature generally observed for the dusty torus (Jaffe et al. 2004). The archival data from the NASA/IPAC Extragalactic Database (NED) are shown in green in Figure 4. The radio observation may be contaminated by the core emission and emissions from other extended region and hence does not satisfy the model curve. The model fitting parameters are given in Table 3. We note that the parameters obtained from our modeling of the broadband SED of these two sources

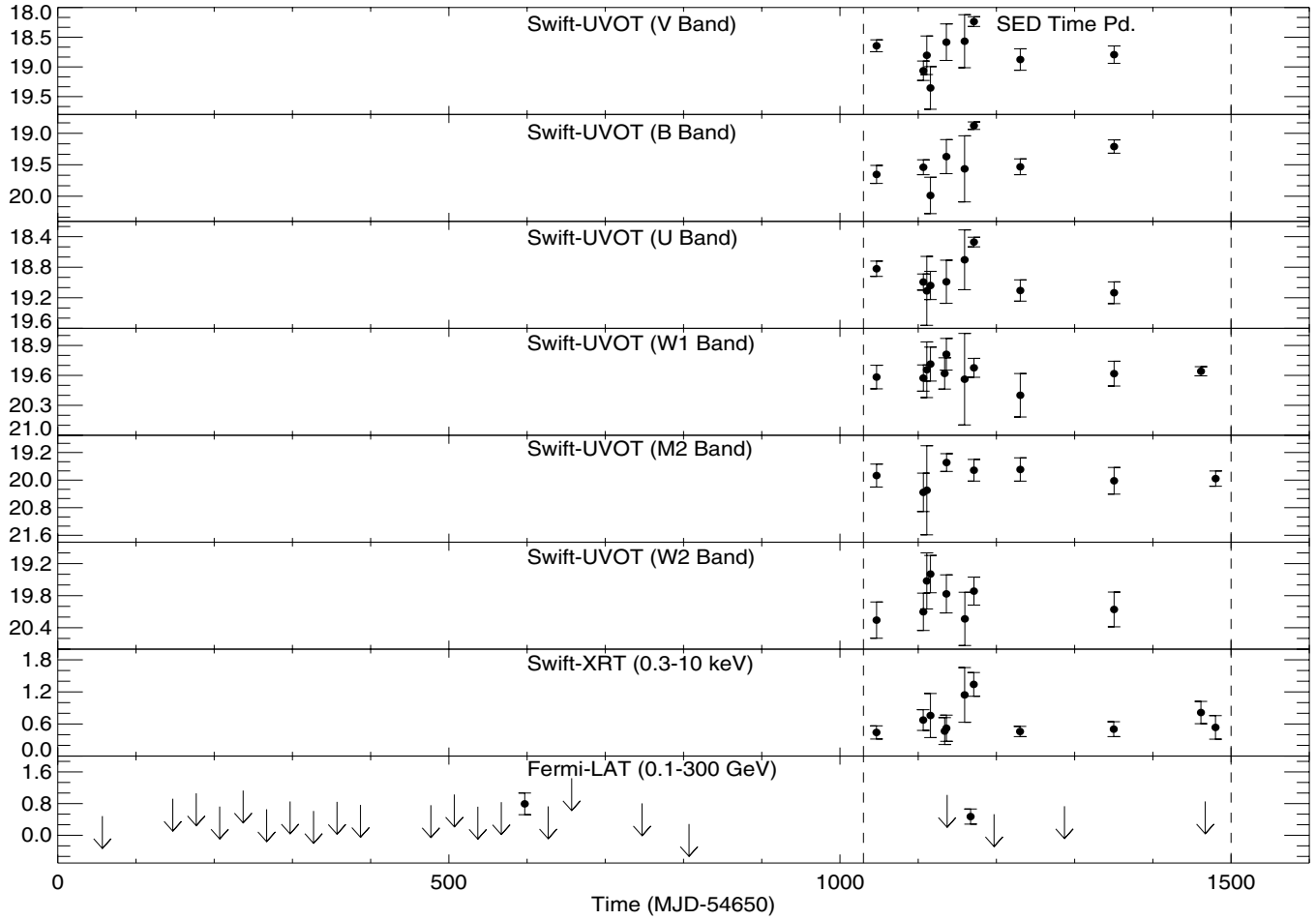

Figure 2. Multi-band light curves of PKS 2004−447. UVOT data are in magnitude. XRT fluxes are in units of 10^{-12} erg cm^{-2} s^{-1}, while LAT γ-ray data have the unit of 10^{-7} photons cm^{-2} s^{-1}. Here, 95% upper limits are shown by vertical arrows. The vertical dashed lines indicate the period for which SED has been made.

Table 2
Summary of SED Analysis

Fermi-LAT							
Source	Time Covered[a]	Flux[b]	Photon Index[c]	Test Statistic[d]			
PKS 1502+036	55800−56130	2.1 ± 0.31	2.93 ± 0.19	87.17			
PKS 2004−447	55680−56130	0.71 ± 0.19	2.93 ± 0.30	19.17			
Swift-XRT							
Source	Time Covered[a]	Exp.[e]	Γ[f]	Flux[g]	Normalization[h]	Stat.[i]	
PKS 1502+036	56042−56103	14.58	1.88 ± 0.22	2.88 ± 0.72	5.28 ± 0.82	14.26/21	
PKS 2004−447	55696−56130	45.89	1.53 ± 0.09	6.26 ± 0.73	8.14 ± 0.57	36.69/37	
Swift-UVOT							
Source	Time Covered[a]	v[j]	b[j]	u[j]	$uvw1$[j]	$uvm2$[j]	$uvw2$[j]
PKS 1502+036	56042−56130	6.54 ± 1.26	5.08 ± 0.82	4.56 ± 0.48	4.53 ± 0.40	3.61 ± 0.51	5.47 ± 0.32
PKS 2004−447	55696−56130	6.59 ± 0.52	4.84 ± 0.34	3.35 ± 0.23	1.62 ± 0.02	1.18 ± 0.12	1.21 ± 0.02

Notes.
[a] Time covered for analysis, in MJD.
[b] Integrated γ-ray flux in the 0.2–300 GeV energy range in units of 10^{-8} photons cm^{-2} s^{-1}.
[c] Photon index calculated from γ-ray analysis.
[d] Significance of detection using likelihood analysis.
[e] Net exposure in kiloseconds.
[f] Photon index of a power-law model.
[g] Observed flux in units of 10^{-13} erg cm^{-2} s^{-1}, in the 0.3–10 keV energy band.
[h] Normalization at 1 keV in 10^{-5} photons cm^{-2} s^{-1} keV^{-1}.
[i] Statistical parameters: χ^2/dof.
[j] Average flux in the *Swift* *V*, *B*, *U*, *W*1, *M*2, and *W*2 bands, respectively, in units of 10^{-13} erg cm^{-2} s^{-1}.

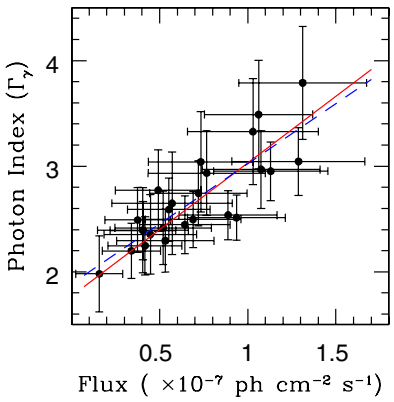

Figure 3. γ-ray photon flux vs. photon index for the source PKS 1502+036. The dashed line (blue) shows the unweighted least-squares fit and the solid line (red) shows the weighted least-squares fit.

(A color version of this figure is available in the online journal.)

differ from the parameters obtained for the same sources by Abdo et al. (2009c). This is primarily due to the inclusion of the simultaneous data corresponding to the synchrotron and SSC component in our SED modeling. These fluxes along with the equipartition condition are sufficient to constrain the main governing parameters of our model.

5. DISCUSSION

Aligned relativistic jets are invoked to explain the extreme power generated by the blazar class of AGNs, with a large fraction of the power being emitted in the γ-ray band. RL-NLSy1 galaxies also have many observed characteristics similar to blazars, namely, flat/inverted radio spectra, the compact core–jet structure on very long baseline interferometry scales (Giroletti et al. 2011; Orienti et al. 2012), high brightness temperature, superluminal jet components (Doi et al. 2006), INOV (Paliya et al. 2013; Liu et al. 2010), and rapid infra-red flux variability (Jiang et al. 2012). However, the detection of variable γ-ray emission in five RL-NLSy1 galaxies (Abdo et al. 2009b, 2009c; D'Ammando et al. 2012; Calderone et al. 2011) clearly shows that NLSy1 galaxies could also have relativistic jets similar to the blazars hosted in elliptical galaxies. If the NLSy1 galaxies are hosted in spiral galaxies, then we should revisit the paradigm that jets can only be launched in elliptical galaxies

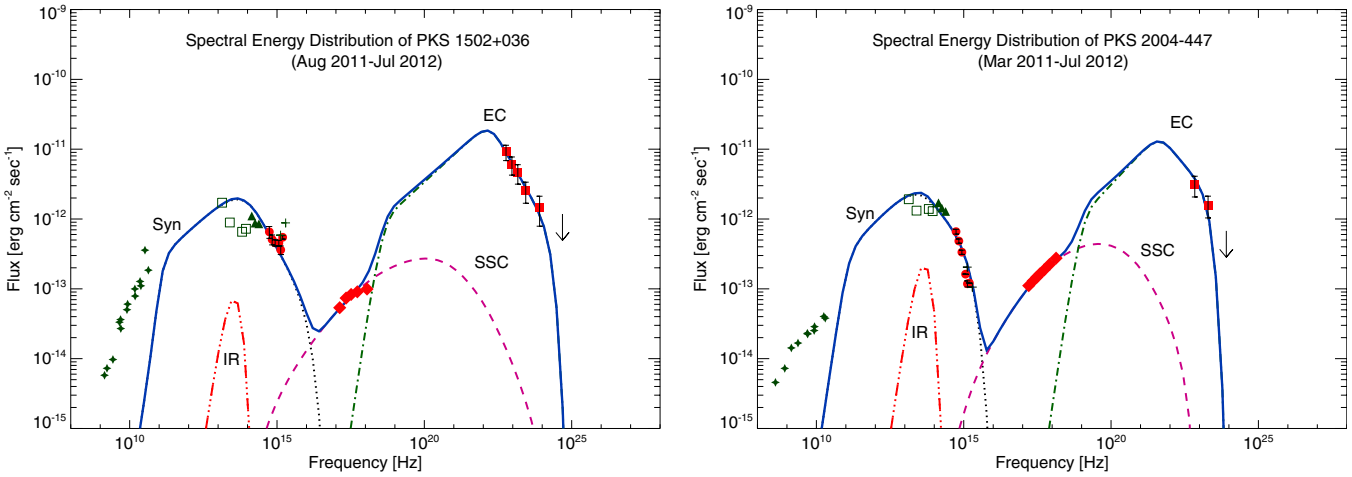

Figure 4. SEDs of γ-NLSy1 galaxies PKS 1502+036 and PKS 2004−447. Flux due to *Fermi*-LAT (filled squares), *Swift* XRT (filled diamonds), and UVOT (filled circles) are indicated with red symbols. The vertical arrow shows the upper limit of γ-ray flux. Archival data are shown in green: 2MASS (upward triangles; Skrutskie et al. 2006), WISE (open squares; Wright et al. 2010), *Galaxy Evolution Explorer* (plus sign; Martin et al. 2005), and radio (filled star; NED). The dotted black line shows synchrotron emission. The SSC (pink) and EC (green) processes are shown by dashed and dotted-dashed lines, respectively. Black body radiation (IR), which is assumed as a reservoir of seed photons for EC, is shown by the orange triple dotted-dashed line. The blue continuous line is the sum of all radiative components. Around 10^{11} Hz, synchrotron self-absorption is clearly visible.

(A color version of this figure is available in the online journal.)

Table 3
Summary of Model Parameters for the SED of PKS 1502+036 and PKS 2004−447

Parameter	Symbol	PKS 1502+036	PKS 2004−447
Redshift	z	0.409	0.240
Particle spectral index (low energy)	p	2.22	2.10
Particle spectral index (high energy)	q	4.5	4.00
Magnetic field (equipartition)	B	0.60 G	0.72 G
Bulk Lorentz factor	Γ	12	9
Comoving emission region size	R'	2.86×10^{16} cm	2.32×10^{16} cm
IR dust temperature in AGN frame	T^*	605 K	694 K
IR torus energy density in AGN frame	u^*	1.02×10^{-3} erg cm^{-3}	1.75×10^{-3} erg cm^{-3}
IR blackbody luminosity in AGN frame	L^*	8.19×10^{43} erg s^{-1}	6.26×10^{43} erg s^{-1}
Particle energy density	U_e	1.43×10^{-2} erg cm^{-3}	2.06×10^{-2} erg cm^{-3}
Minimum electron Lorentz factor	$\gamma'_{\rm min}$	30	60
Break electron Lorentz factor	γ'_b	1870	1176
Maximum electron Lorentz factor	$\gamma'_{\rm max}$	1.8×10^4	7.5×10^3
Jet power	P_j	3.1×10^{45} erg s^{-1}	8.5×10^{44} erg s^{-1}

Table 4
Summary of the Comparison Source Analysis

Fermi-LAT									
Source	Time Covered	Flux	Photon Index	Test Statistic					
3C 454.3	55680−56130	4.9 ± 0.29	2.61 ± 0.06	742.73					
Mrk 421	55680−56130	11.4 ± 0.27	1.79 ± 0.02	10971.46					
Swift-XRT									
Source	Time Covered	Exp.	$N_{\rm H}$	$\alpha^{\rm a}$	$\beta^{\rm a}$	Γ	Flux[b]	Normalization[c]	Stat.
3C 454.3	55729−55924	17.41	6.58	...	...	1.49 ± 0.05	$(6.54 \pm 0.38) \times 10^{-12}$	$(8.43 \pm 0.35) \times 10^{-4}$	86.77/74
Mrk 421	55621−56078	112.4	1.91	2.308 ± 0.001	0.437 ± 0.004	...	$(3.42 \pm 0.01) \times 10^{-10}$	$(8.96 \pm 0.01) \times 10^{-2}$	1177.25/675
Swift-UVOT									
Source	Time Covered	$v^{\rm d}$	$b^{\rm d}$	$u^{\rm d}$	$uvw1^{\rm d}$	$uvm2^{\rm d}$	$uvw2^{\rm d}$		
3C 454.3	55729−55924	7.13 ± 0.13	6.94 ± 0.10	7.46 ± 0.13	7.63 ± 0.16	9.28 ± 0.16	6.59 ± 0.13		
Mrk 421	55621−56078	132.98 ± 4.34	...	156.31 ± 8.24	167.59 ± 1.04	183.96 ± 8.48	169.82 ± 9.91		

Notes. See Table 2 for the description of the remaining parameters.
[a] Log-parabola model parameters used in XSPEC.
[b] 0.3–10 keV flux, in units of erg cm^{-2} s^{-1}.
[c] Normalization having units as photons cm^{-2} s^{-1} keV^{-1}.
[d] *Swift* *V*-, *B*-, *U*-, *W*1-, *M*2-, and *W*2-band fluxes in units of 10^{-12} erg cm^{-2} s^{-1}.

(Marscher 2009). The blazar-like behavior shown by these γ-NLSy1 galaxies, powered by smaller mass black holes and accreting close to the Eddington limit, also poses questions about their nature vis-a-vis blazars and their place in the traditional blazar sequence. Thus, an understanding of these sources will enable one to probe jet physics at a different mass range compared to blazars. We have presented here a detailed analysis of two such RL-NLSy1 galaxies, namely, PKS 1502+036 and PKS 2004−447 using multi-wavelength data and modeling. Our multi-wavelength light curves clearly show the objects to be variable; however, owing to the sparseness of the data, correlations if any on the flux variations between different frequency bands could not be ascertained.

From the modeling of the SEDs of both PKS 1502+036 and PKS 2004−447, using the one-zone leptonic model of Sahayanathan & Godambe (2012), we find that for these sources, the UV-optical data are well fit with synchrotron emission, the X-ray data are fit with SSC, and the γ-ray points are fit with EC scattering of IR photons from the torus. The power of the jet estimated from the fit parameters is larger for PKS 1502+036 compared to PKS 2004−447. To see how the SEDs of these two γ-NLSy1 galaxies match with that of blazars, we also built two other SEDs, one for the well-studied FSRQ 3C 454.3 ($z = 0.859$) and the other for the BL Lac Mrk 421 ($z = 0.030$). For both 3C 454.3 and Mrk 421, we utilized data that covered the same period as that used for the two γ-NLSy1 galaxies studied here. The data for both 3C 454.3 and Mrk 421 were analyzed using the procedures outlined in Section 3, except for the XRT analysis of Mrk 421 wherein we have used a log-parabola model (Massaro et al. 2004a, 2004b). The results of the spectral analysis for 3C 454.3 and Mrk 421 are given in Table 4. In Figure 5, we show the SEDs of PKS 1502+036 and PKS 2004−447 along with the FSRQ 3C 454.3 and BL Lac Mrk 421. In this figure too, the archival data are from NED and BZCAT.[7] We found that during the period considered for spectral analysis, 3C 454.3 was in a quiescent state while Mrk 421 was in an exceptionally bright state.

From Figure 5, it is clear that for 3C 454.3, the synchrotron emission peaks in the IR region, whereas the high-energy EC emission peaks in the MeV–GeV range. However, for Mrk 421, the synchrotron emission peaks in the UV−X-ray spectral band and the high-energy SSC emission peaks in the GeV–TeV region. While the optical/UV luminosities of the two γ-NLSy1 galaxies are comparable to that of Mrk 421, their γ-ray luminosities are significantly higher than the flaring Mrk 421. This clearly demonstrates that SSC alone cannot account for the high-energy emission from these two γ-NLSy1 galaxies and that EC is needed. Such an EC model is frequently invoked to explain the high-energy emission from FSRQs (Dermer et al. 1992; Sikora et al. 1994, 2009). In the powerful FSRQ PKS 1510−089, based on the observed coincidence of γ-ray flux to the appearance of new knots, Marscher et al. (2010) hint that the γ-rays are produced from a region well beyond the radius of the BLR, most likely in the IR torus. Thus, the high-energy emission from these γ-NLSy1 galaxies clearly resembles that of FSRQs and likely due to IC scattering of IR photons from the dusty torus. Another supporting fact for the above-mentioned theory is that the nominal temperature of the molecular torus is about ∼300 K (Landt et al. 2010) to ∼1200 K (Cleary et al. 2007; Malmrose et al. 2011) with a hot emitting region expected to be nearer to the central supermassive black holes. The IR torus temperature that we obtained from SED analysis is about ∼600–700 K for both sources, which means that the dissipation region may lie outside the BLR. Recently, Zhang et al. (2012) have also noted that the observed broadband SEDs of four NLSy1 galaxies detected by *Fermi* are in close resemblance to FSRQs than BL Lac objects. In the SEDs of these NLSy1 galaxies (see Figure 5), it is clear that the low-energy bump is in the IR regime, while the high-energy bump is in the MeV–GeV band. Also, it is clear from Figure 5 that both the low- and high-energy peaks of these γ-NLSy1 galaxies are intermediate to that of 3C 454.3 and Mrk 421. Thus, both PKS 1502+036 and PKS 2004−447 (and maybe other γ-NLSy1 galaxies) could fit very well into the traditional blazar sequence (Fossati et al. 1998; Foschini et al. 2010).

Recently, Chen & Bai (2011) have reported that the γ-NLSy1 galaxies occupy the low-luminosity–low-frequency region in the synchrotron peak frequency (ν_s)–luminosity (L_s) plane. This trend can also be seen very well in Figure 5, where L_s of both PKS 1502+036 and PKS 2004−447 are similar to that

[7] http://www.asdc.asi.it/bzcat/

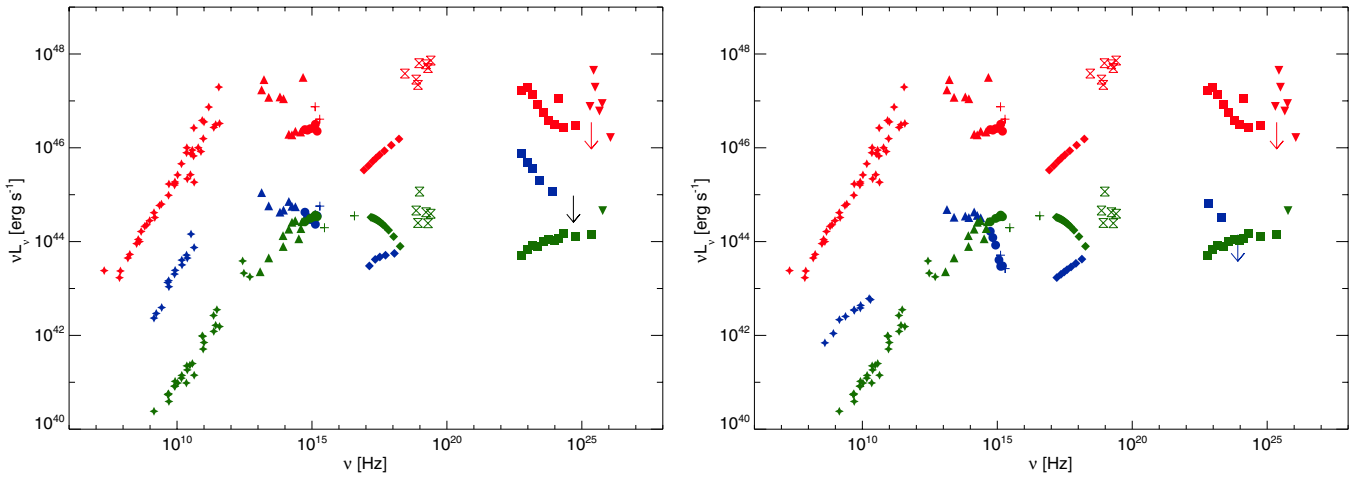

Figure 5. SEDs of γ-NLSy1 galaxies PKS 1502+036 (left panel) and PKS 2004−447 (right panel) along with that of 3C 454.3 and Mrk 421. Spectral data points of γ-NLSy1 galaxies are shown with blue colors. Data points of 3C 454.3 (upper side of the plot) and Mrk 421 (lower side of the plot) are shown with red and green colors, respectively. Vertical arrows show the upper limit of *Fermi*-LAT γ-ray flux. *Fermi*-LAT data are shown with filled squares, while *Swift* XRT and UVOT data are shown with filled diamonds and filled circles, respectively. Archival radio data are shown with filled stars, whereas IR, UV, and hard X-ray data are shown with filled upward triangles, plus sign, and hourglass, respectively. Filled downward triangles show the MAGIC (Anderhub et al. 2009) upper limit data of 3C 454.3 and HAGAR (Shukla et al. 2012) data of Mrk 421.

(A color version of this figure is available in the online journal.)

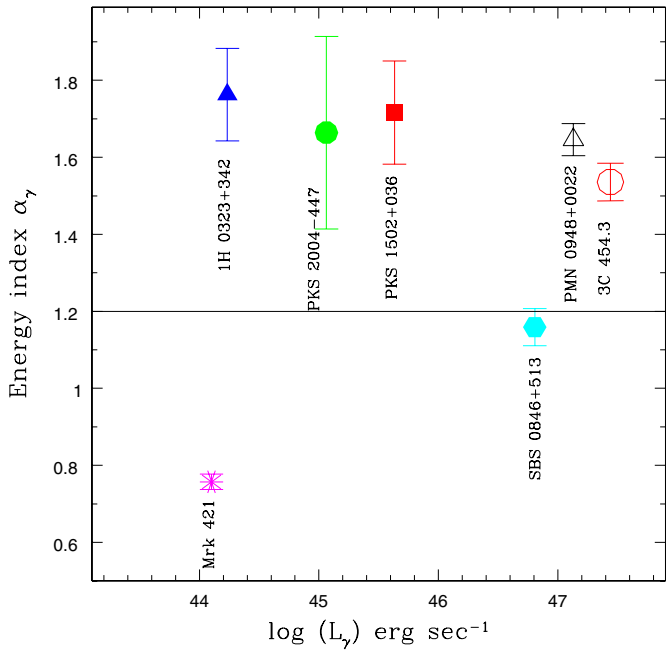

Figure 6. Spectral index (α_γ) vs. luminosity (L_γ) in the energy band 0.1–10 GeV. The horizontal gray line marks $\alpha_\gamma = 1.2$.

(A color version of this figure is available in the online journal.)

of Mrk 421, whereas their corresponding peak frequencies are quite different. Both of them have ν_s in the lower frequency region compared to Mrk 421. Again, the possible explanation for such low-luminosity–low-frequency behavior of both PKS 1502+036 and PKS 2004−447 could be due to their low black hole masses (Chen & Bai 2011; Ghisellini & Tavecchio 2008).

In Figure 6, we have shown the position of the two NLSy1 galaxies studied here in the γ-ray spectral index versus *K*-corrected γ-ray luminosity plane along with the FSRQ 3C 454.3 and the BL Lac Mrk 421. Also shown in Figure 6 are the other three known γ-NLSy1 galaxies, namely, 1H 0323+342 ($z = 0.063$), SBS 0846+513 ($z = 0.584$), and PMN J0948+0022 ($z = 0.584$). The *K*-corrected γ-ray luminosities were evaluated following Ghisellini et al. (2009). Considering only the sources studied here, namely, PKS 1502+036 and PKS 2004−447, we find that their γ-ray luminosities are intermediate to the FSRQ 3C 454.3 and BL Lac Mrk 421, and they have a steep γ-ray spectral index similar to FSRQs (Ghisellini et al. 2009). However, considering all the *Fermi*-detected NLSy1 galaxies up to now, we found that they have a wide range of γ-ray luminosities overlapping the region occupied by BL Lac objects and FSRQs (Ghisellini et al. 2009, 2011); however, the steep γ-ray spectral index displayed by most of them leads us to argue that in terms of the γ-ray spectral index behavior, *Fermi*-detected NLSy1 galaxies are similar to FSRQs.

Further, as discussed by Costamante (2009), FSRQs are more Compton-dominated (Compton dominance is the ratio between Compton and synchrotron luminosities, CD $\equiv L_C/L_s$) than BL Lac objects and on average show a sequence of values from $\sim$100 in FSRQs to $\lesssim$1 in high-energy-peaked BL Lac objects (HBLs). If we calculate CD for our sources, then it comes to $\sim$10 for both of them. Finally, X-ray spectra of low-energy-peaked BL Lac objects (LBLs) and FSRQs are believed to be dominated by IC emission of low-energy electrons and thus a flat spectral index ($\alpha_x < 1$) is expected. As we move from LBL to HBL sources, the peak shifts toward higher energies and the tail of the synchrotron emission starts to dominate, and a steep spectrum ($\alpha_x > 1$) is expected. If we calculate the X-ray spectral indices for our sources (see Tables 2 and 4), then we find that both PKS 1502+036 and PKS 2004−447 have flat spectral indices (0.88 and 0.53, respectively), which are intermediate to 3C 454.3 (0.49) and Mrk 421 (1.31).

Thus, from an analysis of the presently available multi-wavelength data set of PKS 1502+036 and PKS 2004−447, we find that many of their properties are intermediate to the FSRQ 3C 454.3 and the BL Lac Mrk 421. Further, our analysis also suggests that these sources may be low black hole mass counterparts of powerful FSRQs. However, we caution that as of now, there is no unambiguous observational evidence for these two sources in particular and NLSy1 galaxies in general to be hosted by spiral galaxies having low-mass black holes.

However, going by the present widely considered notion that NLSy1 galaxies are powered by low-mass black holes in spiral galaxies, the current observational evidence for the presence of aligned jets in the NLSy1 galaxies detected by *Fermi* goes against the prevailing idea of jets being launched only by elliptical galaxies. A clear picture of the nature of these sources will emerge when more observations become available in the future.

6. CONCLUSIONS

In this work, we have analyzed the two intermediate redshifted γ-NLSy1 galaxies using all available data covering the IR, optical, UV, X, and γ-ray regimes to understand their physical characteristics. We also compare the results obtained with two other well-studied sources, namely, the FSRQ 3C 454.3 and the BL Lac Mrk 421. We arrive at the following conclusions.

1. The broadband SEDs of PKS 1502+036 and PKS 2004−447, although less powerful, resemble more the SEDs of the FSRQ class of AGNs. A possible interpretation is that they could be the low black hole mass counterparts of powerful FSRQs. However, the potential connection between NLSy1 galaxies and FSRQs needs further detailed investigation.
2. The Compton dominance and the X-ray spectral index of PKS 1502+036 and PKS 2004−447 are between the values found for 3C 454.3 and Mrk 421. In the γ-ray luminosity–spectral index plane, these sources have luminosities intermediate to those of 3C 454.3 and Mrk 421; however, they have a steep γ-ray spectral index similar to the FSRQ 3C 454.3. Including the other three γ-NLSy1 galaxies (see Figure 6), we found that γ-NLSy1 galaxies may have a wider range of γ-ray luminosities between FSRQs and BL Lac objects; however, they have a γ-ray spectral index more like FSRQs. The derived spectral properties of the two sources studied here are, in general, similar to blazars and intermediate between the FSRQ 3C 454.3 and BL Lac Mrk 421. They thus could fit well into the traditional blazar sequence.
3. In the γ-ray band, the spectral "softening when brightening" trend is clearly seen for PKS 1502+036. A similar trend is also seen in PKS 2004−447 between the available two epochs of observations. This is against the "harder when brighter" trend seen in the FSRQ 3C 454.3.

We thank the anonymous referee for critical comments which helped in the improvement of the manuscript. This research has made use of data from the OVRO 40 m monitoring program (Richards et al. 2011) which is supported in part by NASA grants NNX08AW31G and NNX11A043G, and NSF grants AST-0808050 and AST-1109911. This research has made use of the data obtained from the High Energy Astrophysics Science Archive Research Center (HEASARC) provided by NASA's Goddard Space Flight Center. This research has made use of the NASA/IPAC Extragalactic Database (NED) which is operated by the Jet Propulsion Laboratory, California Institute of Technology, under contract with the National Aeronautics and Space Administration. This research has made use of the XRT Data Analysis Software (XRTDAS) developed under the responsibility of the ASI Science Data Center (ASDC), Italy.

Facilities: Fermi, *Swift*

REFERENCES

Abdo, A. A., Ackermann, M., Ajello, M., et al. 2009a, ApJ, 700, 597
Abdo, A. A., Ackermann, M., Ajello, M., et al. 2009b, ApJ, 699, 976
Abdo, A. A., Ackermann, M., Ajello, M., et al. 2009c, ApJL, 707, L142
Abdo, A. A., Ackermann, M., Ajello, M., et al. 2010a, ApJ, 715, 429
Abdo, A. A., Ackermann, M., Ajello, M., et al. 2010b, ApJ, 710, 1271
Anderhub, H., Antonelli, L. A., Antoranz, P., et al. 2009, A&A, 498, 83
Andruchow, I., Romero, G. E., & Cellone, S. A. 2005, A&A, 442, 97
Arnaud, K. A. 1996, in ASP Conf. Ser. 101, Astronomical Data Analysis Software and Systems V, ed. G. H. Jacoby & J. Barnes (San Francisco, CA: ASP), 17
Atwood, W. B., Abdo, A. A., Ackermann, M., et al. 2009, ApJ, 697, 1071
Barthelmy, S. D., Barbier, L. M., Cummings, J. R., et al. 2005, SSRv, 120, 143
Begelman, M. C., Blandford, R. D., & Rees, M. J. 1984, RvMP, 56, 255
Begelman, M. C., & Sikora, M. 1987, ApJ, 322, 650
Błażejowski, M., Sikora, M., Moderski, R., & Madejski, G. M. 2000, ApJ, 545, 107
Boettcher, M., Mause, H., & Schlickeiser, R. 1997, A&A, 324, 395
Boller, T., Brandt, W. N., & Fink, H. 1996, A&A, 305, 53
Burrows, D. N., Hill, J. E., Nousek, J. A., et al. 2005, SSRv, 120, 165
Calderone, G., Foschini, L., Ghisellini, G., et al. 2011, MNRAS, 413, 2365
Calderone, G., Ghisellini, G., Colpi, M., & Dotti, M. 2012, arXiv:1212.1181
Cardelli, J. A., Clayton, G. C., & Mathis, J. S. 1989, ApJ, 345, 245
Cash, W. 1979, ApJ, 228, 939
Chen, L., & Bai, J. M. 2011, ApJ, 735, 108
Cleary, K., Lawrence, C. R., Marshall, J. A., Hao, L., & Meier, D. 2007, ApJ, 660, 117
Costamante, L. 2009, IJMPD, 18, 1483
D'Ammando, F., Orienti, M., Finke, J., et al. 2012, MNRAS, 426, 317
Dermer, C. D., & Schlickeiser, R. 1993, ApJ, 416, 458
Dermer, C. D., Schlickeiser, R., & Mastichiadis, A. 1992, A&A, 256, L27
Doi, A., Nagai, H., Asada, K., et al. 2006, PASJ, 58, 829
Doi, A., Nagira, H., Kawakatu, N., et al. 2012, ApJ, 760, 41
Foschini, L. 2011, in Proceedings of Science, vol. 126, Narrow-Line Seyfert 1 Galaxies and their Place in the Universe, ed. L. Foschini, M. Colpi, L. Gallo et al. (Pos(NLS1)024), pos.sissa.it/cai-bin/reader/conf_cai?confid=126
Foschini, L., Fermi/Lat Collaboration, Ghisellini, G., et al. 2010, in ASP Conf. Ser. 427, Accretion and Ejection in AGN: a Global View, ed. L. Maraschi, G. Ghisellini, R. Della Ceca, & F. Tavecchio (San Francisco, CA: ASP), 243
Fossati, G., Maraschi, L., Celotti, A., Comastri, A., & Ghisellini, G. 1998, MNRAS, 299, 433
Gallo, L. C., Edwards, P. G., Ferrero, E., et al. 2006, MNRAS, 370, 245
Gehrels, N., Chincarini, G., Giommi, P., et al. 2004, ApJ, 611, 1005
Ghisellini, G., Celotti, A., Fossati, G., Maraschi, L., & Comastri, A. 1998, MNRAS, 301, 451
Ghisellini, G., & Madau, P. 1996, MNRAS, 280, 67
Ghisellini, G., & Maraschi, L. 1989, ApJ, 340, 181
Ghisellini, G., Maraschi, L., & Tavecchio, F. 2009, MNRAS, 396, L105
Ghisellini, G., & Tavecchio, F. 2008, MNRAS, 387, 1669
Ghisellini, G., & Tavecchio, F. 2009, MNRAS, 397, 985
Ghisellini, G., Tavecchio, F., Foschini, L., & Ghirlanda, G. 2011, MNRAS, 414, 2674
Giommi, P., Padovani, P., Polenta, G., et al. 2012, MNRAS, 420, 2899
Giroletti, M., Paragi, Z., Bignall, H., et al. 2011, A&A, 528, L11
Goodrich, R. W. 1989, ApJ, 342, 224
Grupe, D., & Mathur, S. 2004, ApJL, 606, L41
Hayashida, K. 2000, NewAR, 44, 419
Healey, S. E., Romani, R. W., Taylor, G. B., et al. 2007, ApJS, 171, 61
Jaffe, W., Meisenheimer, K., Röttgering, H. J. A., et al. 2004, Natur, 429, 47
Jiang, N., Zhou, H.-Y., Ho, L. C., et al. 2012, ApJL, 759, L31
Kalberla, P. M. W., Burton, W. B., Hartmann, D., et al. 2005, A&A, 440, 775
Kimball, A. E., Ivezić, Ž., Wiita, P. J., & Schneider, D. P. 2011, AJ, 141, 182
Komossa, S., Voges, W., Xu, D., et al. 2006, AJ, 132, 531
Konigl, A. 1981, ApJ, 243, 700
Landt, H., Buchanan, C. L., & Barmby, P. 2010, MNRAS, 408, 1982
Leighly, K. M. 1999a, ApJS, 125, 297
Leighly, K. M. 1999b, ApJS, 125, 317
Liu, H., Wang, J., Mao, Y., & Wei, J. 2010, ApJL, 715, L113
Malmrose, M. P., Marscher, A. P., Jorstad, S. G., Nikutta, R., & Elitzur, M. 2011, ApJ, 732, 116
Marscher, A. P. 2009, arXiv:0909.2576
Marscher, A. P., & Gear, W. K. 1985, ApJ, 298, 114
Marscher, A. P., Jorstad, S. G., Larionov, V. M., et al. 2010, ApJL, 710, L126
Martin, D. C., Fanson, J., Schiminovich, D., et al. 2005, ApJL, 619, L1
Massaro, E., Perri, M., Giommi, P., & Nesci, R. 2004a, A&A, 413, 489

Massaro, E., Perri, M., Giommi, P., Nesci, R., & Verrecchia, F. 2004b, A&A, 422, 103
Mattox, J. R., Bertsch, D. L., Chiang, J., et al. 1996, ApJ, 461, 396
Maune, J. D., Miller, H. R., & Eggen, J. R. 2013, ApJ, 762, 124
Melia, F., & Konigl, A. 1989, ApJ, 340, 162
Murphy, T., Sadler, E. M., Ekers, R. D., et al. 2010, MNRAS, 402, 2403
Orienti, M., D'Ammando, F., Giroletti, M., & for The Fermi-LAT Collaboration, 2012, arXiv:1205.0402
Oshlack, A. Y. K. N., Webster, R. L., & Whiting, M. T. 2001, ApJ, 558, 578
Osterbrock, D. E., & Pogge, R. W. 1985, ApJ, 297, 166
Paliya, V. S., Stalin, C. S., Kumar, B., et al. 2013, MNRAS, 428, 2450
Peterson, B. M., McHardy, I. M., Wilkes, B. J., et al. 2000, ApJ, 542, 161
Poole, T. S., Breeveld, A. A., Page, M. J., et al. 2008, MNRAS, 383, 627
Pounds, K. A., Done, C., & Osborne, J. P. 1995, MNRAS, 277, L5
Press, W. H., Teukolsky, S. A., Vetterling, W. T., & Flannery, B. P. 1992, Numerical Recipes in C. The Art of Scientific Computing (Cambridge: Cambridge Univ. Press)
Richards, J. L., Max-Moerbeck, W., Pavlidou, V., et al. 2011, ApJS, 194, 29
Roming, P. W. A., Kennedy, T. E., Mason, K. O., et al. 2005, SSRv, 120, 95
Sahayanathan, S., & Godambe, S. 2012, MNRAS, 419, 1660
Shukla, A., Chitnis, V. R., Vishwanath, P. R., et al. 2012, A&A, 541, A140
Sikora, M., Begelman, M. C., & Rees, M. J. 1994, ApJ, 421, 153
Sikora, M., Stawarz, Ł., Moderski, R., Nalewajko, K., & Madejski, G. M. 2009, ApJ, 704, 38
Skrutskie, M. F., Cutri, R. M., Stiening, R., et al. 2006, AJ, 131, 1163
Stickel, M., Padovani, P., Urry, C. M., Fried, J. W., & Kuehr, H. 1991, ApJ, 374, 431
Stocke, J. T., Morris, S. L., Gioia, I. M., et al. 1991, ApJS, 76, 813
Urry, C. M., & Padovani, P. 1995, PASP, 107, 803
Véron-Cetty, M.-P., & Véron, P. 2010, A&A, 518, A10
Wagner, S. J., & Witzel, A. 1995, ARA&A, 33, 163
Wang, T., Brinkmann, W., & Bergeron, J. 1996, A&A, 309, 81
Wright, E. L., Eisenhardt, P. R. M., Mainzer, A. K., et al. 2010, AJ, 140, 1868
Xu, D., Komossa, S., Zhou, H., et al. 2012, AJ, 143, 83
Yuan, W., Zhou, H. Y., Komossa, S., et al. 2008, ApJ, 685, 801
Zhang, J., Sun, X. N., Zhang, S. N., & Liang, E. W. 2012, in IAU Symposium, vol. 290, Feeding Compact Objects: Accretion on All Scales, ed. C. M. Zhang, T. Belloni, M. Mendez, & S. N. Zhang, 359
Zhou, H., Wang, T., Yuan, W., et al. 2006, ApJS, 166, 128